Electron Spin-Lattice Relaxation Processes of Radicals in Irradiated Crystalline Organic Compounds

James R. Harbridge, Sandra S. Eaton, and Gareth R. Eaton*

Department of Chemistry and Biochemistry, University of Denver, Denver, Colorado 80208-2436

Received: June 27, 2002; In Final Form: October 23, 2002

Electron spin-lattice relaxation times (T_{1e}) for the major radicals in γ-irradiated polycrystalline samples of glycylglycine, L-alanine, 2,4,6-tri-*tert*-butyl-phenol, and 4-methyl-2,6-di-*tert*-butyl-phenol were measured as a function of temperature using pulsed EPR. CW-saturation recovery (CW-SR) were obtained at X-band (9.1 GHz) and S-band (3.0 GHz) between about 10 and 295 K. Inversion recovery, echo-detected saturation recovery (ED-SR), and pulsed electron−electron double resonance (ELDOR) curves were obtained at X-band between 77 and about 295 K. For 2,4,6-tri-*tert*-butyl-phenoxy radical, which has a single-line EPR spectrum, the recovery times obtained by the three methods were in good agreement and were assigned as T_{1e}. For the three radicals with resolved hyperfine splitting, spectral diffusion caused the recovery times observed by inversion recovery or ED-SR to be significantly shorter than T_{1e} obtained by CW-SR or ELDOR. Spectral diffusion processes were observed directly by pulsed ELDOR experiments, and time constants for cross relaxation and nuclear relaxation were obtained by modeling the ELDOR curves. For irradiated L-alanine and for the 4-methyl-2,6-*tert*-butyl-phenoxy radical at some temperatures, the effects of rapid cross relaxation on CW-SR curves could not be fully mitigated even by long saturating pulses, and T_{1e} could only be determined by ELDOR. For the radicals in γ-irradiated L-alanine, 2,4,6-tri-*tert*-butyl-phenol, and 4-methyl-2,6-di-*tert*-butyl-phenol, methyl group rotation makes significant contributions to T_{1e} at temperatures where the rate of rotation of a methyl group is comparable to the microwave frequency. Activation energies for methyl rotation were determined by modeling the temperature dependence of T_{1e} at X-band and S-band. In temperature ranges where methyl rotation did not dominate, T_{1e} was dominated by Raman, direct, or local mode processes.

Introduction

Electron spin relaxation times reflect the environment of the paramagnetic species and can be used to obtain a wide variety of information, including insights into electronic structure, dynamic processes, and distances between centers with differing relaxation times.[1] To obtain reliable values of the electron spin-lattice relaxation time, T_{1e}, it is necessary to understand how other relaxation processes may contribute to experimental data obtained by various techniques. One goal of these studies was to compare inversion recovery, echo-detected saturation recovery (ED-SR) with a 6 μs saturating pulse, long-pulse continuous wave saturation recovery (CW-SR), and electron−electron double resonance (ELDOR) methods of measuring T_{1e}. The second goal of this study was to characterize the effects of strongly and weakly coupled methyl groups on T_{1e} and on spectral diffusion processes that impact recovery curves. The effects of methyl groups on nuclear spin relaxation have been extensively studied by NMR,[2−7] but the effects on electron spin relaxation have been much less thoroughly examined.

Spin-lattice relaxation requires transfer of energy from the spins to the surroundings. In the direct process there is a match of the Zeeman energy with a phonon energy, so that there can be a direct transfer of energy from the spin system to the lattice phonon bath. The direct process often dominates spin-lattice relaxation at temperatures below about 10 K.[1a,8−14] The Raman process is a two-photon process in which the Zeeman energy is equal to the difference between the energies absorbed and emitted for a virtual excited state with an energy that is less than the Debye temperature.[1,8−10,15] The Raman process has been found to dominate spin-lattice relaxation for some $S = 1/2$ systems in glassy matrixes or magnetically dilute solids between 10 and 200 K.[1a,16] Thermally activated dynamic processes, including methyl group rotation, amino group rotation, or movement of a hydrogen-bonded proton, can absorb energy from the spin system when the frequency of the process is comparable to the electron Larmor frequency.[2−7,17,18] Other processes that may contribute to electron spin relaxation are Orbach-Aminov processes[19] and local vibrational modes.[19−21] The mechanisms by which these processes affect spin-lattice relaxation include modulation of hyperfine interaction,[22] of spin−orbit coupling,[23,24] or of zero-field splitting.[25]

If the experimental recovery curve at a particular temperature fits well to a single exponential, a single process dominates the relaxation. However, in many cases the recovery curves do not fit well to a single exponential, which can arise from orientation dependence of T_{1e} in polycrystalline samples, a distribution in T_{1e}, and/or contributions from spectral diffusion processes. Spectral diffusion is a broad term that encompasses all processes that transfer spin polarization from one position in the spectrum to another.[1a] A variety of spectral diffusion processes have been described in the literature.[1a,26−39] Nuclear spin relaxation is a spectral diffusion process ($\Delta M_s = 0$, $\Delta M_I = \pm 1$) that transfers spin polarization from one nuclear spin state to another. Cross-relaxation transfers spin polarization between Zeeman frequen-

* Corresponding author. Phone: 303-871-2980. Fax: 303-871-2254. E-mail: geaton@du.edu.

10.1021/jp021504h CCC: $25.00
Published on Web 01/10/2003

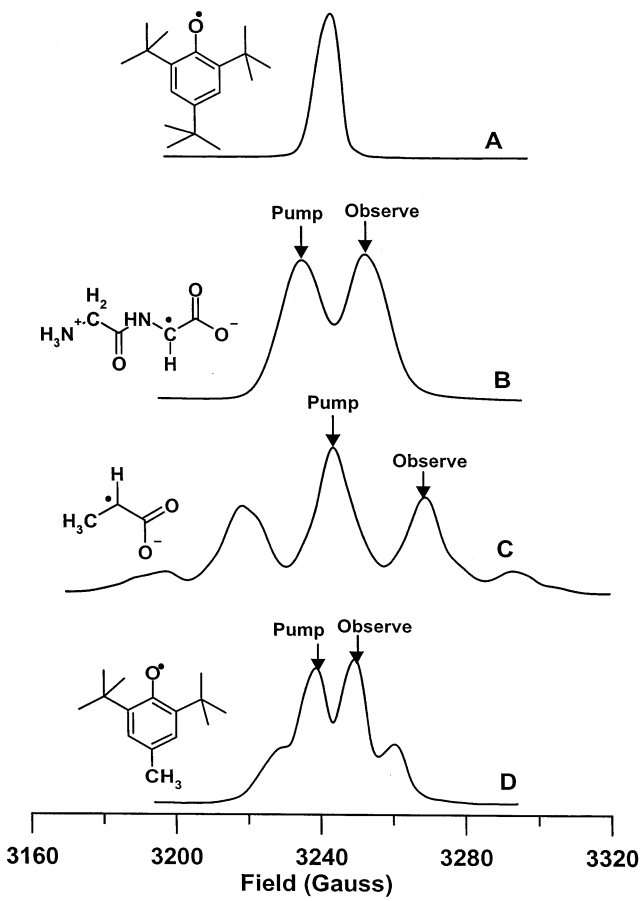

Figure 1. Room-temperature integrated CW absorption spectra of the four radicals in polycrystalline samples studied. Spectra were obtained at X-band with 0.5 G modulation amplitude and 100 kHz modulation frequency. The positions of the excitation and observing pulses for ELDOR experiments are shown. **A**: 2,4,6-*t*-Bu-phenoxide radical, **B**: glycylglycine radical, **C**: irradiated L-alanine, **D**: 4-Me-2,6-*t*-Bu-phenoxide radical.

cies by processes that involve mutual flip of two unlike spins. In the present discussion, cross relaxation is used to designate spectral diffusion processes in which $\Delta M_s = \pm 1$, $\Delta M_I = \mp 1$. Pulsed electron−electron double resonance (ELDOR), with the pump and observe pulses on different hyperfine lines, can be used to determine the time constants for cross-relaxation and for nuclear relaxation processes involving flip of a nuclear spin that gives rise to resolved hyperfine splitting. Spin diffusion moves magnetization between unresolved hyperfine components within an inhomogeneously broadened line.[1a]

To evaluate the effectiveness of methods for measuring T_{1e} in samples with various spectral diffusion processes, radicals with different proton hyperfine coupling patterns were selected (Figure 1). The EPR spectrum (Figure 1A) of the radical in irradiated 2,4,6-tri-*tert*-butyl-phenol (2,4,6-*t*-Bu-phenol) is a single line with unresolved hyperfine coupling to the ring protons and to the *tert*-butyl methyl protons.[40] The EPR spectrum of the radical in irradiated glycylglycine (Figure 1B) exhibits resolved coupling to a single proton with $A_H \sim 18$ G.[41,42] The room-temperature EPR spectrum of the dominant stable radical in irradiated L-alanine (Figure 1C) exhibits approximately equal coupling (~25 G) to a unique proton and to the protons of a methyl group. For the radical in irradiated 4-methyl-2,6-di-*tert*-butyl-phenol (4-Me-2,6-*t*-Bu-phenol), the coupling to the three equivalent protons of the 4-methyl group in the fast methyl-rotation regime is about 11 G.[17,18,43,44] Comparison of the relaxation processes for the radical in L-alanine and for the 4-Me-2,6-*t*-Bu-phenoxy radical with those for the 2,4,6-*t*-Bu-phenoxy radical shows the differences between the effects on T_{1e} of methyl protons that give resolved hyperfine splittings and more weakly coupled methyl protons.

Materials and Methods

Samples. Polycrystalline samples of glycylglycine (Aldrich, Milwaukee, WI), L-alanine (Sigma, St. Louis, MO), 2,4,6-*t*-Bu-phenol (97$^+$%, Aldrich), and 4-Me-2,6-*t*-Bu-phenol (99$^+$%, Aldrich) were irradiated at room temperature with a ^{60}Co source to a dose of approximately 6 MRad. A single crystal of L-alanine was irradiated with a dose of approximately 12 MRad. After irradiation, samples were stored in air at room temperature. Experiments were performed weeks to months after irradiation, and no evidence of significant radical degradation was observed. Spin concentrations were determined by comparison of double-integrated first-derivative CW spectra with spectra for a 0.53 mM solution of 2,2,6,6-tetramethyl-piperidinyl-1-oxy (Aldrich Chemical Co., Milwaukee, WI) in toluene. The radical concentrations in these irradiated solids are the following: glycylglycine, 7.2×10^{18} spins/cm^3; L-alanine, 1.3×10^{19} spins/cm^3; 2,4,6-*t*-Bu-phenol, 6.7×10^{17} spins/cm^3; and 4-Me-2,6-*t*-Bu-phenol, 2.2×10^{18} spins/cm^3. On the basis of measurements with several aliquots of L-alanine in typical Wilmad Glass Company (Buena, NJ) 4 mm EPR tubes, the mass of sample per column height in the tube and the estimated diameter of the tube indicate that the packing of the solid results in about 0.8 g/cm^3. Using this approximate conversion factor, the L-alanine sample contained about 2×10^{19} spins/g, which is in reasonable agreement with the literature value for a dose of 6 MRad (6×10^4 Gy).[45]

Except at low temperatures where the direct process dominates, T_{1e} is expected to be independent of electron spin concentration.[1a] For samples of L-alanine irradiated at about 6 and 20 MRad, the spin concentrations were 1.3×10^{19} and 2.5×10^{19} spins/cm^3. Samples of glycylglycine irradiated at about 2.3, 6, and 24 MRad had spin concentrations of 3.6×10^{18}, 7.2×10^{18}, and 2.1×10^{19} spins/cm^3, respectively. For both radicals, CW-SR curves at 295 K for samples with different radiation doses were indistinguishable. As discussed below, the CW-SR curves for these samples are dominated by T_{1e}, with some contribution from T_{x1} for irradiated L-alanine. Unlike T_{1e}, spin diffusion is likely to depend on the spin packet width, which can be measured by electron spin−echo spectroscopy. If spin−echo decay is dominated by electron−electron dipolar interactions, it would be concentration dependent.[46] Two-pulse spin−echo studies showed that echo decays for these irradiated solids were dominated by dynamic processes that averaged inequivalent environments, or by nuclear spin diffusion.[47] Thus, at the spin concentrations present in these samples, spin packet widths are not dependent on electron spin concentration. Therefore for each solid, a sample at a single radiation dose was deemed to be sufficient to distinguish T_{1e} from other processes that contribute to the recovery curves.

Spectroscopy. X-band (ca. 9.1 GHz) CW-SR measurements were made using a locally constructed spectrometer.[48] Temperatures between 10 and 70 K were obtained using an Oxford ESR900 flow cryostat. Temperature at the sample, as a function of liquid helium flow and heater setting, was calibrated by replacing the sample with a tube containing a thermocouple immersed in 1:1 water/glycerol. The temperature at the sample was strongly dependent upon the helium flow rate, which causes

as much as 2 K uncertainty in the temperature. Temperatures between 77 and 230 K were obtained using a Varian liquid nitrogen cooled gas flow system. Temperatures above 230 K were obtained by flowing N_2 gas through a coil submersed in a dry ice−acetone bath. Between 77 and 300 K, the temperature was measured with a thermocouple near the top of the sample, and the uncertainty in sample temperature is less than 1 K. The CW-SR data were acquired in the limit where the saturation recovery time constant was independent of increasing pump time.

S-band (ca. 3.0 GHz) CW-SR curves were acquired on a locally built spectrometer[49] equipped with a crossed-loop resonator (CLR) that is similar to a previously described resonator.[50] The CLR assembly, including the first-stage amplifier, was in a custom-built CryoIndustries (Atkinson, NH) cryostat with two thermocouples attached to the resonator for sample temperature measurement. Temperatures from 77 to 250 K were obtained by flowing N_2 gas through a coil submersed in liquid nitrogen. Temperatures below 77 K were obtained by liquid helium flow. A Conductus LTC 10 controller was used for temperature regulation.

X-band pulsed ELDOR, inversion recovery, ED-SR, and spin−echo data were acquired on a locally built spectrometer equipped with a 1 kW pulsed TWT, a TE_{102} cavity resonator, and a quartz dewar insert.[51,52] The resonator was over-coupled to $Q \sim 120$ to 150. The samples were cooled by nitrogen gas flowing through a coil submersed in liquid nitrogen. A Wavetek MicroSweep model 965 was the frequency source for the first pulse of the 3-pulse experiments. A pair of General Microwave PIN diode SP2T switches (F9120AH, rise and fall times of 10 ns, 60 dB isolation) was used to rapidly switch between the two frequency sources. For the pulsed ELDOR experiments, the pump (ν_2) and observe (ν_1) frequencies were set symmetrically about the frequency of the resonator to generate similar B_1 for the pump and observe pulses. A 180° pulse was 64 ns long. The pulse sequence for inversion recovery and inversion ELDOR (IE) was 180°-τ-90°-T-180°-T-echo in which τ was varied and $T = 160$ ns was the time between the end of the second pulse and the beginning of the third pulse. The first 180° pulse was at ν_1 or ν_2, for the inversion recovery or inversion ELDOR experiments, respectively. The second and third pulses were at ν_1. The pulse sequence for ED-SR and saturation ELDOR (SE) was (low-power 6 μs pulse)-τ-90°-T-180°-T-echo. The first pulse was at ν_1 or ν_2, for the ED-SR or saturation ELDOR experiments, respectively. The positions in the CW absorption spectra that were at resonance for the pump and observe pulses for most of the ELDOR experiments are marked in Figure 1. For glycylglycine, the two hyperfine lines are broad enough that additional experiments were performed with the pump and observe ELDOR pulses positioned on the same hyperfine line. The inversion recovery and ED-SR data were obtained at the positions in the spectrum labeled "observe" (Figure 1). Corrections for instrumental artifacts were performed by subtraction of data obtained with the Wavetek turned off. In the absence of an ELDOR effect, a pulse at ν_2 has minimal effect on echo intensity at ν_1. An ELDOR enhancement or reduction is the ratio of the echo intensity at ν_1 following a pulse at ν_2, relative to the echo intensity without a preceding pulse at ν_2.

ELDOR data were not obtained at S-band because the resonator could not be overcoupled to low enough Q to permit ELDOR frequencies corresponding to two resolved hyperfine lines into the resonator. Also, the 20 W TWT that was available at S-band could not excite a large enough bandwidth for the ELDOR experiment.

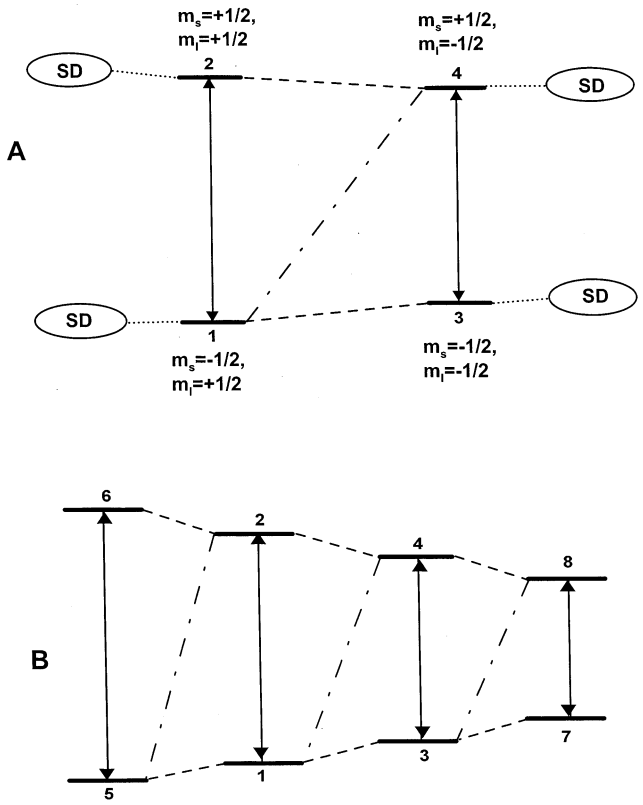

Figure 2. A: Eight-level model used to simulate the pulsed ELDOR curves for the glycylglycine radical, including 4 levels for spin diffusion baths (SD). **B**: Energy level model used to simulate the pulsed ELDOR curves for irradiated L-alanine and 4-Me-2,6-*t*-Bu-phenoxide radical. Each of the eight levels (1−8) has a relaxation pathway for spin diffusion (not shown) that produced a 16-level model. For the ELDOR experiments transition 1 → 2 was pumped and transition 3 → 4 was observed. For inversion recovery and ED-SR experiments, transition 3 → 4 was excited and observed. Time constants T_{1e} (−), T_{1n} (- - -), T_{x1} (− · −), and T_s (···) were adjusted to obtain the best fits to the experimental data.

Analysis of the Pulsed EPR Data. The CW-SR, ED-SR, and inversion recovery curves were analyzed first by fitting to a single exponential using a Levenberg-Marquardt algorithm. For curves that fit well to a single exponential, the uncertainty in the time constant is about 10%. Provencher's Multifit routine[53] was used to fit the data to the sum of exponentials, and distinctions between single and multiple exponential fits were based on the statistical tests in the program. The relative weightings for multiple exponential components also were analyzed using Brown's UPEN routines.[54,55] However, even for recovery curves with high signal-to-noise ratios, the time constants obtained from these analyses showed substantial scatter and dependence on the length of the data acquisition window. As the contributions from faster components become larger, it is increasingly difficult to extract reliable values of T_{1e}. For example, for irradiated alanine, the values of T_{1e} obtained by CW-SR are significantly longer than the "slow" component that was obtained previously from an inversion recovery study of irradiated L-alanine by fitting data to the sum of exponentials.[56]

For the glycylglycine radical, an 8-level model was used to analyze the contributions of relaxation processes to the ELDOR curves (Figure 2A). In the inversion recovery or saturation recovery experiments, transition 3 → 4 is both excited and

observed. In the ELDOR experiments, transition 1 → 2 is excited by the first pulse and transition 3 → 4 is observed. Four relaxation times were used to model the return of the spin system to equilibrium. T_{1e} equilibrates levels that differ only in M_s. T_{1n} equilibrates levels that differ only in M_I. T_{x1} is the cross relaxation process with $\Delta M_s + \Delta M_I = 0$ ($\Delta M_s = \pm 1$, $\Delta M_I = \mp 1$). T_{x2} ($\Delta M_s + \Delta M_I = \pm 2$) was assumed to be significantly longer than T_{x1},[57] and was not included in the model. Four additional levels are connected to levels 1−4 by spin diffusion with time constant T_s (Figure 2A).

For the radicals in L-alanine and 4-Me-2,6-*t*-Bu-phenol, there are more than two resolved hyperfine lines so the model in Figure 2A was extended to include the hyperfine lines to high-field and low-field of the transitions that were pumped and observed (Figure 2B). In addition to the 8 levels shown in Figure 2B, there are 8 corresponding levels (not shown) that are connected by spin diffusion to levels 1−8. For L-alanine, the lowest field line (∼3195 G in Figure 1) was not included in the simulation because it was assumed that it made a negligible contribution to relaxation for transition 3−4. The relative intensities of the hyperfine lines were used to calculate the probabilities of nuclear spin flips between pairs of adjacent hyperfine lines. It was assumed that the relative populations of spins excited and observed were proportional to the line intensities. For irradiated L-alanine at 298 K, these assumptions were tested by pumping on each of the transitions and observing either of the adjacent transitions. The observed magnitude of the ELDOR enhancement for each pair of lines was proportional to that calculated based on the probabilities of spin flips and relative line intensities. It was assumed that all spins in adjacent lines could be characterized by the same values of T_{x1} or T_{1n}. If this is not the case, it would be a systematic source of error.

To analyze the inversion recovery and inversion ELDOR curves, Mathcad (MathSoft, Cambridge, MA) routines were written based on the models in Figure 2A and 2B. The time dependence of the population of each level was expressed in terms of the four time constants and the deviation of the instantaneous population from the equilibrium Boltzmann population.[58,59] The resulting equations for the 8-level model are given in the Appendix. The evolution of the populations was calculated using numerical integration with a fourth-order Runge-Kutte algorithm. The populations of the levels that are involved in the transition that was excited by the first pulse were adjusted to match the extent of inversion observed immediately following the pulses. Complete inversion was not attained, which may be due to incomplete excitation of the inhomogeneously broadened lines. T_{1e}, T_{x1}, T_{1n}, and T_s were adjusted iteratively to simultaneously give the best fit of the calculated signals to the experimental inversion recovery and inversion-ELDOR curves. Curves initially were modeled assuming negligible spin diffusion. In the temperature regions where inversion recovery experiments demonstrated the importance of spin diffusion, T_s and the populations of the spin bath levels were adjusted to account for the fastest component in the inversion recovery curve and for the magnitude of the ELDOR reduction or enhancement. The estimated uncertainty in T_{1e}, T_{x1}, and T_{1n} is about 10% except at temperatures where two or more time constants are similar, and therefore are difficult to distinguish.

In the ELDOR measurements the pump pulse on transition 1 → 2 (Figure 2) decreases the population of level 1 and increases the population of level 2. Observation of an ELDOR reduction for transition 3 → 4 indicates that the population of level 3 is low and/or the population of level 4 is high, which can occur if nuclear spin relaxation transfers magnetization between levels 1 and 3 and between 2 and 4 more rapidly than other relaxation processes. Thus, the observation of an ELDOR reduction indicates that $T_{1n} < T_{1e}$, T_{x1}.

Observation of an ELDOR enhancement indicates that the population of level 3 is high and/or the population of level 4 is low, which arises when cross relaxation occurs more rapidly than other relaxation processes. Thus the observation of an ELDOR enhancement indicates that $T_{x1} < T_{1e}$, T_{1n}. The diagrams in Figure 2 are drawn assuming that $A_H > 0$. If $A_H < 0$, then T_{x1} would connect levels 2 and 3, but short T_{x1} would still result in an ELDOR enhancement.

In the inversion ELDOR experiment, hard (nonselective) pulses were used for the pump and observe pulses, so the fraction of the "pumped" line that is excited is comparable to the fraction of the "observed" line that is detected. This results in a relatively well-defined initial state for the observed magnetization. In the saturation ELDOR experiments, the initial long low-power saturating pulse is relatively selective. Although $B_1 = 0.2$ to 0.6 G, the 6 μs length of the pulse means that $1/t_p$ is ∼0.06 G, which excites a small fraction of the "pumped" line. The shorter observing pulses had B_1 about 3 G, which excites a substantial fraction of the "observe" line. This results in a less well-defined initial state for the observed magnetization, which complicates quantitative modeling of the data. T_{1e}, T_{x1}, and T_{1n} obtained by fitting saturation ELDOR curves were consistent with values obtained from inversion ELDOR curves. However, the Mathcad routines were not successful in modeling the magnitude of the enhancements or reductions in the saturation ELDOR curves, which is attributed to an incomplete description of the events that occur during the long saturating pulses.

Analysis of the Temperature Dependence of T_{1e}. The temperature dependence of $1/T_{1e}$ was fitted to

$$\frac{1}{T_{1e}} = A_{dir}T + A_{Ram}\left(\frac{T}{\theta_D}\right)^9 J_8\left(\frac{\theta_D}{T}\right) + A_{loc}\left(\frac{e^{\Delta_{loc}/T}}{(e^{\Delta_{loc}/T}-1)^2}\right) + A_{Me}\left[\frac{2\tau_c}{1+\omega^2\tau_c^2}\right] \quad (1)$$

where T is the temperature in Kelvin, A_{dir} is the coefficient for the contribution from the direct process, A_{Ram} is the coefficient for the Raman process, θ_D is the Debye temperature, J_8 is the transport integral,

$$J_8\left(\frac{\theta_D}{T}\right) = \int_0^{\theta_D/T} x^8 \frac{e^x}{(e^x-1)^2}\mathrm{d}x$$

A_{loc} is the coefficient for the contribution from a local vibrational mode, Δ_{loc} is the energy for the local mode in Kelvin, A_{Me} is the coefficient for the contribution from thermally activated methyl rotation, τ_c is the correlation time which is equal to $\tau_o e^{E_a/kT}$, E_a is the activation energy, and τ_o is the preexponential factor. An Orbach process was not considered because there are no known low-lying electronic states for the radicals examined. Mathematical expressions for the temperature dependence of spin-lattice relaxation are taken from the following references: Raman process,[60,61] local mode,[20] and thermally activated process.[62]

Strategy Used in Analyzing Temperature Dependence of T_{1e}. For each sample, the temperature dependence of T_{1e} was fitted with the smallest number of contributing processes consistent with the experimental data. Comparison of data at

TABLE 1: Contributions to Spin-Lattice Relaxation Determined by Fitting to eq 1[a]

irradiated solid	temperature range studied (K)	direct A_{dir} (s^{-1} K^{-1})	Raman A_{Ram} (s^{-1}), θ_D (K)	local A_{loc} (s^{-1}), Δ_{loc} (K)	methyl rotation[c] E_a (K), τ_0 (s), ϵ^b, A_{therm} (X), A_{therm}(S) (s^{-2})
2,4,6-*t*-Bu-phenol	25 to 295		4.3×10^4, 150	2×10^6, 1000	800, 7×10^{-12}, 0.6, 1.3×10^{15}, 7×10^{14}
glycylglycine	16 to 295	0.5	1.8×10^4, 140	2×10^5, 1120	
L-alanine	16 to 330	5.5	2.0×10^4, 150		1450, 7×10^{-15}, 0.85, 2.5×10^{15}, 2×10^{15}
4-Me-2,6-*t*-Bu- phenol	13 to 295				165, 3×10^{-13}, 0.68, 8×10^{14}, 4×10^{14}

[a] Energies in Kelvin. To convert from Kelvin to kJ/mol, multiply by 8.37×10^{-3}. [b] Davidson-Cole distribution parameter.[63] [c] Contributions from a second thermally activated methyl rotation process are not included in the table. Values from the literature were used as discussed in text.

X-band and S-band distinguished between the effects on T_{1e} due to methyl rotation, which is frequency dependent, and contributions from other processes that are not frequency dependent. In temperature ranges where methyl rotation dominates, there are two adjustable parameters, τ_0 and E_a. The uncertainties in these parameters are decreased by requiring agreement with the data at both microwave frequencies. Distributions of activation energies were used to model the contribution of methyl rotation to T_{1e}. A Gaussian distribution or a Fang distribution[63] did not give as good fits to the temperature dependence of $1/T_{1e}$ as a Davidson-Cole distribution.[63] In the Fang distribution, interaction with the lattice leads to increased steric hindrance and there is a distribution of activation energies above a lower limit value. In the Davidson-Cole distribution there is an upper limit on the activation energy and a distribution below that limit. This model has been widely used to interpret nuclear spin relaxation in solids.[63] In temperature ranges where methyl rotation did not dominate spin-lattice relaxation, a Raman process and/or local vibrational mode dominated T_{1e}. The Raman process typically dominates at lower temperatures than local vibrational modes and results in a smaller slope in a plot of $\log(1/T_{1e})$ versus $\log(T)$ than local vibrational modes. Table 1 summarizes the parameters that were used to obtain the fit lines for the X-band and S-band data. Parameters for a second thermally activated methyl rotation process that contributes above about 250 K for irradiated L-alanine and above about 150 K for 4-Me-2,6-*t*-Bu-phenol were not included in Table 1 because of large uncertainties in the values. T_{1e} data were not obtained at high enough temperatures to encompass the high-temperature limits for these processes, so literature values for E_a were used to calculate the fit lines in these regions.

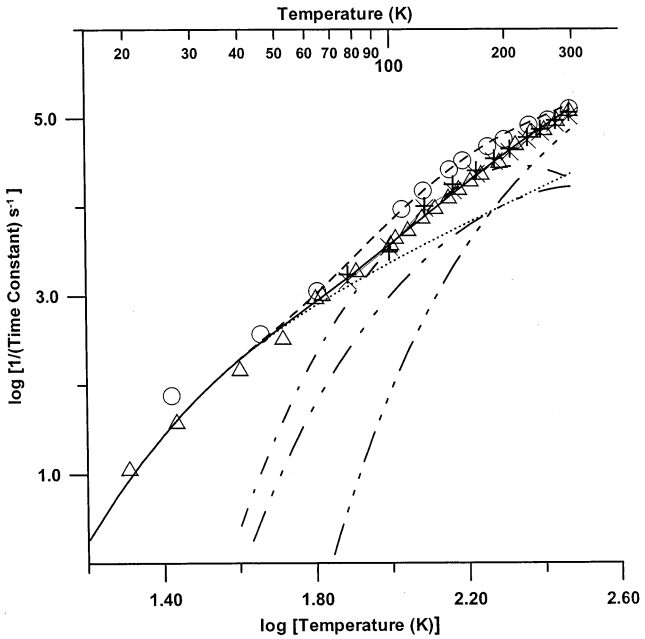

Figure 3. Temperature dependence of the recovery rate constants obtained for 2,4,6-*t*-Bu-phenoxy radical by (+) X-band inversion recovery with $B_1 = 3.0$ G, (×) X-band ED-SR, (△) X-band CW-SR, and (○) S-band CW-SR. The parameters for the fits to the (−) X-band and (- - -) S-band CW-SR are summarized in Table 1. Contributions from (•••) Raman process, (− • −) methyl rotation at S-band, (− • • −) methyl rotation at X-band, and (− • • • −) local mode are shown.

Results

Time constants obtained as a function of temperature by (a) CW-SR using a pump time that was long relative to T_{1e}, (b) ED-SR with a saturating pulse of 6 μs, and (c) inversion recovery using an initial pulse of 64 ns were compared to determine the contribution of spectral diffusion. Pulsed ELDOR data were used to determine the time constants for nuclear relaxation and cross-relaxation between resolved hyperfine lines and to separate these contributions from T_{1e}. By comparison of the results from the various experiments, a consistent set of spin relaxation time constants was obtained for each sample. The temperature dependence of T_{1e} was modeled to determine the processes that dominate the spin-lattice relaxation. CW-SR data were obtained at two different frequencies to test for thermally activated dynamic processes. Results for each sample are discussed in the following paragraphs.

2,4,6-Tri-*tert*-butyl-phenol. The 2,4,6-*t*-Bu-phenoxy radical is produced by γ-irradiation of 2,4,6-*t*-Bu-phenol.[64] The EPR spectrum (Figure 1A) is a single line with a width at half-height of about 7 G. At X-band inversion recovery, ED-SR and CW-SR gave similar time constants between 77 and 295 K (Figure 3) and the recovery curves fit well to single exponentials. S-band CW-SR curves also fit well to a single exponential. Variation of the microwave B_1 from 6.0 to 1.5 G had little impact on the X-band inversion recovery time constant. These results indicate that spectral diffusion processes make negligible contributions to the recovery curves for this radical, and the time constants are attributed to T_{1e}.

Temperature Dependence of T_{1e}. From 30 to about 60 K, the spin-lattice relaxation times are similar at S-band and X-band, and the temperature dependence of $1/T_{1e}$ could be fitted to a Raman process (Figure 3). From 60 to about 250 K, relaxation times are shorter at S-band than at X-band, which indicates a

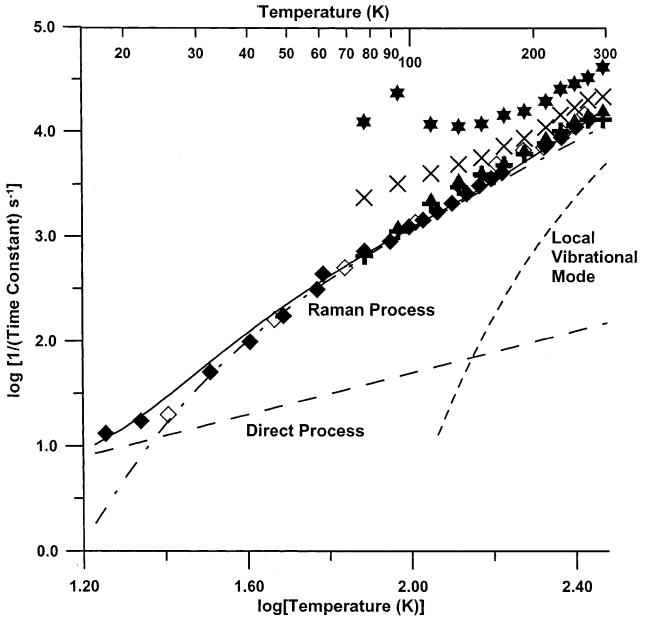

Figure 4. Temperature dependence of the recovery rate constants for the glycylglycine radical obtained from (✱) X-band inversion recovery with $B_1 = 3.0$ G, (×) X-band ED-SR, (+) X-band inversion ELDOR, (▲) X-band saturation ELDOR, (◆) X-band CW-SR, and (◇) S-band CW-SR curves. The fit function (−) for the data obtained by X-band and S-band CW-SR includes contributions from the Raman (− • −), direct (- - -), and local mode (•••) processes. Parameters for the fit line are given in Table 1.

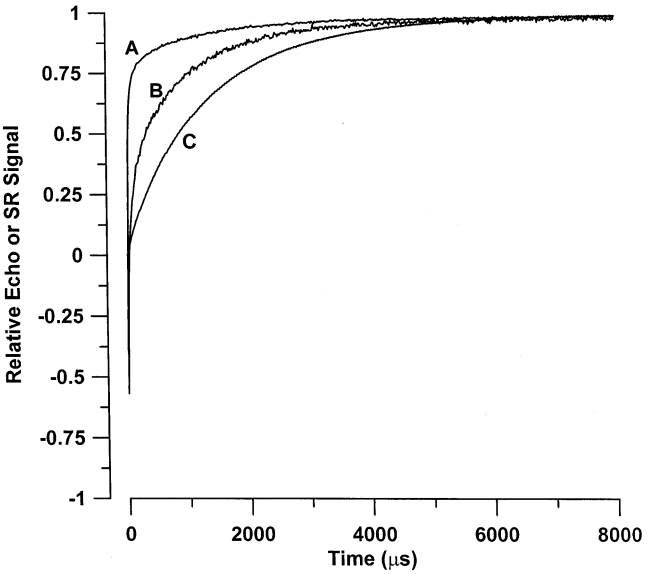

Figure 5. Recovery curves at 77 K for the glycylglycine radical, obtained by (**A**) inversion recovery with $B_1 = 1.5$ G, (**B**) inversion recovery with $B_1 = 6.0$ G, and (**C**) CW-SR.

contribution from methyl rotation, or other thermally activated process. Two-pulse spin−echo dephasing time constants, T_m, were strongly temperature dependent between 77 and 295 K, with minimum values near 125 K at both X-band and S-band. This temperature dependence of T_m is characteristic of radicals in which a dynamic process is occurring at rates comparable to the electron−proton hyperfine (i.e., a few MHz) that is averaged by the motion. For 2,4,6-*t*-Bu-phenoxy radical these dynamic effects are attributed to rotation of the methyl groups. NMR studies have shown that the barriers to rotation of the inequivalent methyl groups in nonirradiated 2,4,6-*t*-Bu-phenol are 6.7 kJ (800 K) and 10 kJ (1200 K).[5] The use of these values of E_a and a Davidson-Cole distribution parameter $\epsilon = 0.6$ gave good fits to the temperature dependence of $1/T_{1e}$ (Figure 3). Since this process makes a relatively small contribution to $1/T_{1e}$, there is substantial uncertainty in the fit-parameters. Above about 250 K there is little frequency dependence of $1/T_{1e}$ and the temperature dependence is consistent with a contribution from a local mode with $\Delta_{loc} = 1000$ K.

Glycylglycine Radical. The free radical produced by γ-irradiation of glycylglycine[41,42] is shown in Figure 1B. Katayama and Gordy calculated that the electron spin density on the −CH carbon is approximately 0.75.[42] The coupling to the −CH proton produces the 19 G doublet splitting that is observed in the CW spectrum. Couplings to other nuclei broaden the two lines. The full width at half-maximum is about 15 G.

Although the recovery curves for the glycylglycine radical obtained by some experiments do not fit well to a single exponential, approximate single-exponential fits were compared to obtain qualitative indications of trends (Figure 4). The time constants estimated as single-component fits increased in the order inversion recovery < ED-SR < CW-SR, which correlates with the increasing lengths of the excitation pulses, t_p; $t_p = 64$ ns for inversion recovery, $t_p = 6$ μs for ED-SR, and $t_p = 50$ μs to a few ms (depending on T_{1e}) for CW-SR. The dependence of the time constant on t_p and the observation that the inversion recovery and ED-SR curves did not fit well to a single exponential indicate that spectral diffusion processes make substantial contributions to the inversion recovery and ED-SR curves, especially at lower temperatures. Above 160 K, the time constants obtained from ED-SR are more similar to the CW-SR time constants than at lower temperatures, which implies that the effects of the spectral diffusion processes above 160 K are largely suppressed by the 6 μs pulse.

The inversion recovery data shown in Figure 4 were obtained with $B_1 = 3.0$ G, which is a small fraction of the line width. Data also were obtained with $B_1 = 1.5$ or 6.0 G. At low temperature, the recovery curves are strongly dependent on B_1 and the time constant is shorter for either inversion recovery experiment than for CW-SR (Figure 5). The inversion recovery curves were analyzed as a sum of exponentials, with the long component fixed at the value of T_{1e} determined by CW-SR. For $B_1 = 6.0$ G, the time constant of the second component was similar to the values of T_{1n} determined by ELDOR (see below). For the smaller values of B_1, particularly at lower temperatures, the time constant for the second component was faster than T_{1n}. The observation of shorter recovery time constants for smaller B_1 implies that spins excited by the pulses exchanged energy with spins within the inhomogeneously broadened line that were not excited by the pulse. This spectral diffusion process is denoted as spin diffusion and dominates the inversion recovery curves when $B_1 = 1.5$ G.

ELDOR was used to characterize the spectral diffusion processes. Between 77 and 295 K inversion ELDOR showed a reduction of echo intensity for the glycylglycine radical (Figure 6). At each temperature examined, the reduction observed by saturation ELDOR (data not shown) was about twice that observed by inversion ELDOR, which is attributed to greater perturbation of spin populations during the 6 μs pump pulse of the saturation ELDOR experiment than during the 64 ns inverting pulse of the inversion ELDOR experiment. The ELDOR reduction indicates that $T_{1n} < T_{1e}$ throughout the temperature range examined. The initial decrease in ELDOR signal is attributed to T_{1n} and the subsequent recovery is attributed to T_{1e}.

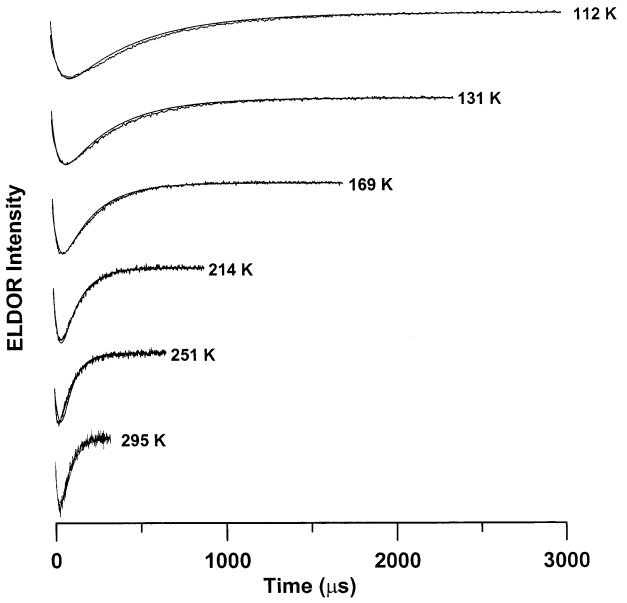

Figure 6. X-band ELDOR curves at selected temperatures for the glycylglycine radical, with simulations using the 8-level model (Figure 2A). The *y*-scale for each curve is 0.88 to 1.00. Throughout the temperature range shown, the ELDOR reduction was about 10%. The parameters for the fit lines are given in the text.

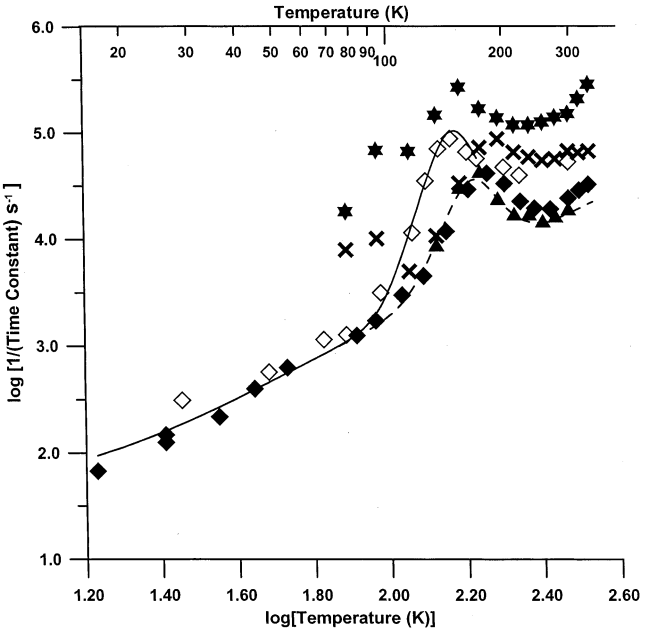

Figure 7. Temperature dependence of the recovery rate constants for irradiated L-alanine from (✱) X-band inversion recovery with B_1 = 3.0 G, (×) X-band ED-SR, (◇) S-band CW-SR, (◆) X-band CW−SR, and (▲) X-band ELDOR curves. The parameters used to fit the (- - -) X-band CW-SR and (−) S-band CW-SR data are summarized in Table 1.

Initial estimates of T_{1e} were obtained by a single-exponential fit to the latter parts of the ELDOR curves and showed that T_{1e} decreases substantially from 77 to 295 K, while T_{1n} showed little temperature dependence (Figure 6). The ELDOR reductions would then be expected to become smaller as the temperature is increased, because the time constants for the two processes become more comparable at higher temperature. However, the ELDOR reductions remained approximately constant throughout the temperature range. To account for this observation, it is proposed that another spectral diffusion process is present, which competes with T_{1n}. On the basis of the B_1 dependence of the inversion recovery curves, this process is attributed to spin diffusion. The inversion recovery and inversion ELDOR recovery curves were simulated with a Mathcad routine that is based on the 8-level model shown in Figure 2A. T_s was about 10 μs between 77 and 295 K. T_{1n} was 40 ± 10 μs between 112 and 295 K. T_{1e} decreased from 430 μs at 77 K to 53 μs at 295 K.

The lines in the spectrum of the glycylglycine radical are wide enough that ELDOR experiments could be performed between positions in the same hyperfine line, with negligible overlap of the pump and observe pulses. At room temperature, saturation ELDOR with a B_1 of about 0.2 G for the pump pulse gave large ELDOR reductions. The time constant for the initial signal reduction is T_s. T_s is of the order of 10 μs and became shorter as the frequency separation between the spins excited by the pump and observe pulses was decreased.

Temperature Dependence of T_{1e}. CW-SR curves at S-band and X-band for the glycylglycine radical were acquired with pulses that were much longer than T_s and T_{1n}, and the curves fit well to a single exponential. The time constants obtained by CW-SR matched well with the time constants obtained by simulation of the ELDOR data, which indicates that the long-pump CW-SR recovery curves were not impacted by spectral diffusion, and so the time constants are assigned as T_{1e}. Between about 30 and 295 K the values of T_{1e} obtained by CW-SR at X-band and S-band are the same (Figure 4), within experimental error, which indicates that the dominant relaxation process is not frequency dependent and thus is not a thermally activated process (eq 1). Between about 30 and 295 K, the temperature dependence of $1/T_{1e}$ could be fitted using a Raman process with a Debye temperature, θ_D, of 140 K. Above about 250 K, there is a small contribution from a local vibrational mode with Δ_{loc} = 1120 K (~800 cm^{-1}) and at temperatures below about 30 K a process with the temperature dependence of a direct process contributes to the relaxation (Figure 4).

L-Alanine. The major free radical produced by γ-irradiation of L-alanine is formed by the removal of the $-NH_3$ group.[65] This radical has been used in radiation dosimeters.[66,67] Relaxation times and methyl dynamics in irradiated L-alanine have been studied using CW-EPR,[18,68] ENDOR,[17,18,57,69] CW-ELDOR,[70] and pulsed EPR.[56,71] The unpaired electron is centered on the carbon that is bonded to the methyl group and a proton (Figure 1C). The average hyperfine coupling to the methyl protons and to the unique proton are approximately equal (~25 G) and give rise to an apparent 5-line EPR spectrum at room temperature (Figure 1B). Although the recovery curves for irradiated L-alanine that were obtained by some experiments at some temperatures did not fit well to a single-exponential, approximate fits were compared to examine trends (Figure 7). Assignment of the multiple time constants that contribute to recovery curves obtained by different methods relied heavily on the ELDOR data, which is described first, followed by a summary of the experimental data divided into three temperature intervals (<100 K, 100 K to 190 K, and 190 K to 330 K).

Analysis of ELDOR Curves. Between 77 and 190 K ELDOR reductions were observed (Figure 8), indicative of $T_{1n} < T_{1e}$. The largest ELDOR reductions (Figure 8) were observed at about 133 K, which is in the temperature range where the rate of methyl rotation is comparable to the average hyperfine coupling to the methyl protons.[68] The reductions observed by saturation ELDOR were up to 7 times as large as by inversion ELDOR, which is attributed to greater perturbation of spin populations during the longer saturating pulses. Above 200 K,

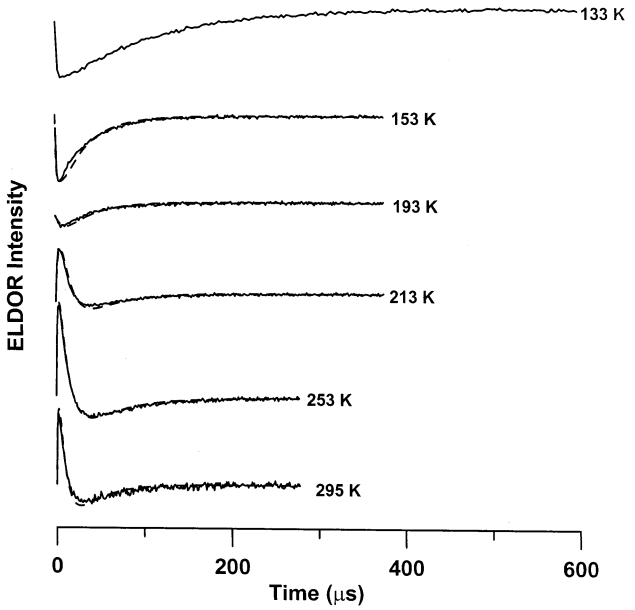

Figure 8. X-band ELDOR curves for irradiated L-alanine at selected temperatures. The *y*-scale for each curve is 0.88 to 1.12. The curve at 253 K shows a 12% enhancement and the curve at 133 K shows a 12% reduction. Simulations (- - -) were calculated based on the model in Figure 2B and the time constants shown in Figure 9.

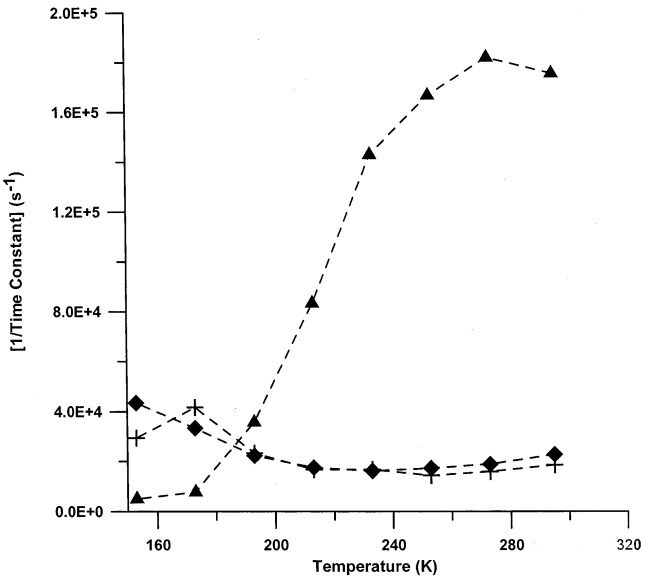

Figure 9. Relaxation rate constants obtained by inversion recovery and inversion ELDOR for irradiated L-alanine: (▲) T_{x1}, (+) T_{1e}, and (◆) T_{1n}. Spin diffusion within the EPR line contributes to the relaxation below 233 K with T_{1s} about 5−10 μs.

an ELDOR enhancement was observed (Figure 8), which indicates $T_{x1} < T_{1n} \leq T_{1e}$. In the ELDOR curves T_{x1} dominates the initial rise; T_{1n} and T_{1e} contribute to the signal decrease and subsequent return to equilibrium. The depth of the reduction is determined by the relative values of T_{1e} and T_{1n}. The 16-level Mathcad model (Figure 2B) is based on the hyperfine splitting pattern in the rapid methyl-rotation limit, so the model was used only to analyze ELDOR data at temperatures above 150 K. The time constants obtained by modeling the ELDOR data are shown in Figure 9. The maximum in $1/T_{x1}$ was at about 273 K, which is in good agreement with the maximum at about 260 K observed by Angelone et al. by LODESR.[57] Below about 213 K, in addition to the time constants shown in Figure 8, spin diffusion with a time constant of about 5−10 μs was needed to account for a rapid component in the inversion recovery curves and to model the magnitude of the ELDOR reduction. Near 180 K, $T_{1e} \sim T_{1n} \sim T_{x1}$ and the ELDOR curves show little enhancement or reduction. The values of T_{1e} obtained by the modeling were in good agreement with values obtained by fitting the latter portions of the ELDOR curves to a single exponential.

Comparison of Time Constants Obtained by Various Methods. CW spectra of irradiated L-alanine show that below about 100 K the rotation of the methyl group is slow enough that hyperfine couplings to inequivalent methyl protons are observed.[68] In this temperature range, CW-SR curves at S-band and X-band fit well to single exponentials and the recovery time constants are the same at the two frequencies. ELDOR reductions were observed at 77 and 93 K, which indicates $T_{1n} < T_{1e}$, and the values of T_{1e} agreed with the values obtained by CW-SR. Inversion recovery curves at 77 and 100 K were strongly dependent on B_1, consistent with $T_s < T_{1e}$. Inversion recovery and ED-SR curves at 77 and 100 K did not fit well to single exponentials due to contributions from T_{1n} and T_s. Thus, in this temperature regime we conclude that reliable values of T_{1e} can be measured by single-exponential fits to CW-SR curves, but not to ED-SR or inversion recovery curves.

As temperature is increased above 110 K, the CW spectra of irradiated L-alanine show that the rate of rotation of the methyl group becomes comparable to the difference between hyperfine couplings to inequivalent methyl protons, and spectra are in the intermediate exchange regime.[68] Above about 160 K, the rate of rotation of the methyl group is fast relative to the inequivalence of electron−proton hyperfine couplings and the methyl protons appear equivalent on the EPR time scale.[68] Up to 180 K at X-band and to 145 K at S-band, CW-SR curves fit well to single exponentials. The time constants at X-band obtained by CW-SR are in good agreement with the values obtained by ELDOR, and so the CW-SR time constants at X-band (up to 180 K) and at S-band (up to 145 K) are attributed to T_{1e}. The inversion recovery curves in this temperature interval are strongly dependent on B_1, consistent with $T_s < T_{1e}$, and the curves do not fit well to a single exponential. Between 110 and 170 K, the time constants obtained by X-band ED-SR are similar to values obtained by CW-SR (Figure 6). In this temperature range it appears that T_{1e} is short enough and the 6 μs pump time in the ED-SR experiment is long enough to mitigate the effects of the spectral diffusion processes that contributed to the inversion recovery curves. Thus, from 100 K up to about 180 K (X-band) or 145 K (S-band), T_{1e} could be determined by CW-SR or ED-SR. At higher temperatures, ELDOR was required to determine T_{1e}.

Above 190 K the time constants obtained from the X-band CW-SR curves are shorter than the time constants obtained from the ELDOR curves. The fast process in the multiexponential recovery of the CW-SR curves in this temperature range is attributed to cross relaxation. It appears that the effects of cross relaxation cannot be fully suppressed by the long saturating pulses in CW-SR. Fitting of the CW-SR curves to the sum of exponentials gave time constants for the long component that were similar to T_{1e} obtained by ELDOR, but with substantial scatter in the values. The inversion recovery curves also exhibit multiple components, but there is little dependence on B_1 above about 215 K, which indicates that T_s is longer than other contributions to the spectral diffusion. Fitting of the inversion recovery curves above 190 K to the sum of two exponentials gave time constants similar to T_{x1} and T_{1e} obtained by ELDOR but with substantial scatter in the values. At 298 K the values of T_{1e} obtained by CW-SR and ELDOR are 41 and 60 μs,

respectively, which are significantly longer than the value of 21.2 μs obtained previously by fitting inversion recovery curves to the sum of two exponentials for a different hyperfine line.[56]

The results in ref 56 were obtained for the low-field line of the 5-line spectrum of a single crystal of irradiated L-alanine. For a single crystal, at a series of orientations that spanned a range of proton hyperfine splittings, T_{1e} measured by ELDOR at 77 or 180 K varied by less than about 20% as a function of orientation or position in the spectrum. The ELDOR reductions were 27% to 80% at 77 K, depending on which lines were pumped or observed, and the resulting recoveries fit well to a single exponential. At both temperatures the values of T_{1e} in the single crystal differ by less than 20% from the values in the polycrystalline sample. By contrast, the spectral diffusion contributions to the recovery curves were strongly dependent on position in the spectrum. For both the single crystal and polycrystalline samples, the contribution from spectral diffusion was substantially larger for the low-field or high-field lines than for the center line, which is attributed to the relative populations of the adjacent lines and corresponding probabilities for spectral diffusion processes. Thus, measurements of T_{1e} for the low-field and high-field lines by techniques other than ELDOR are particularly sensitive to spectral diffusion.

Temperature Dependence of T_{1e}. By combining the data obtained from CW-SR and ELDOR, T_{1e} values were obtained at X-band from 15 to 295 K. ELDOR data were not obtained at S-band, so the extent to which spectral diffusion contributes to the observed recovery curves is not known. By analogy with the X-band data, it is proposed that spectral diffusion contributed to the CW-SR curves above 145 K, where the data did not fit well to a single exponential. At both X-band and S-band, the contributions from spectral diffusion are more significant at temperatures above the value that corresponds to the local maximum in $1/T_{1e}$ (Figure 7), which is the temperature region where T_{x1} is short.

At X-band and S-band below 30 K, T_{1e} is dominated by a relaxation process with a temperature dependence similar to that of the direct process (Figure 7). The bulk spin concentration for the L-alanine sample is about 1×10^{19} spins/cm^3, which is relatively high. Thus, the relaxation observed at this radical concentration at low temperature may have contributions from intermolecular electron spin−spin interactions.[1] Between 30 and 90 K, the relaxation times at X-band and S-band are dominated by a Raman process with a Debye temperature, θ_D, of 150 K. Between 90 and 200 K, the relaxation times are different at X-band and S-band; $1/T_{1e}$ goes through a maximum at about 160 K at S-band and about 190 K at X-band (Figure 7). The frequency and temperature dependence is consistent with domination of T_{1e} by rotation of the methyl groups at rates comparable to the Larmor frequency. The temperature dependence of T_{1e} at both frequencies was fitted with an activation energy, E_a, of 1475 K and Davidson-Cole distribution parameter $\epsilon = 0.85$. For this activation energy the rate of rotation matches the S-band frequency at 162 K and the X-band frequency at 186 K, in good agreement with the experimental data (Figure 7). Activation energies between 1375 and 1600 K produced adequate fits to the temperature dependence of $1/T_{1e}$, so the estimated uncertainty in E_a is about $\pm$100 K. The activation energy of 1475 K (12.3 kJ) is on the low end of literature values, which range from 1475 to 2120 K (12.3 to 17.6 kJ).[17,56,57,68,71]

Above about 160 K there is some uncertainty in the values of T_{1e} at S-band because of the contributions from spectral diffusion. However, even with that uncertainty, it is evident that $1/T_{1e}$ at S-band is faster than at X-band (Figure 7), which indicates that an additional dynamic process dominates the relaxation. The frequency dependence of T_{1e} at room temperature was observed in a prior study,[72] but the dynamic process responsible for the frequency dependence was not assigned. On the basis of the data obtained in this study, we attribute this process to rotation of the lattice methyl groups at rates comparable to the electron Larmor frequency. The lattice methyl groups, which are attached to sp^3 carbons, have higher activation energies than the methyl group attached to an sp^2 carbon in the radical. NMR studies of nonirradiated L-alanine[3] obtained $E_a = 2700$ K (22.4 kJ) for rotation of methyl groups. The use of these activation energies gave a reasonable fit to the X-band data for T_{1e} above 200 K (Figure 7).

4-Methyl-2,6-di-*tert*-butyl-phenol. The 4-Me-2,6-*t*-Bu-phenoxy radical is produced by γ-irradiation of 4-Me-2,6-*t*-Bu-phenol.[73] The unpaired electron spin density is delocalized in the π orbitals of the benzene ring. The spin density on the 4-carbon is about 0.5,[73] and coupling to the protons of the methyl group gives rise to a 4-line EPR spectrum at room temperature (Figure 1D). Below about 20 K, rotation of the methyl groups is slow relative to differences in hyperfine couplings to inequivalent methyl protons.[18]

Analysis of ELDOR Curves. X-band ELDOR experiments were performed between 77 and 295 K. The ELDOR enhancement decreased from about 10% at 77 K to a negligible value above 140 K. The enhancement is attributed to $T_{x1} < T_{1n}, T_{1e}$. The inversion recovery and inversion ELDOR curves between 77 and 112 K were simulated using a Mathcad routine based on the 16-level model in Figure 2B. T_{x1} increased from 11 μs at 77 K to 35 μs at 112 K. T_{1e} was about 300 μs in this temperature range and T_{1n} was about 250 μs. The similarity in values of T_{1e} and T_{1n} makes the analysis more ambiguous. Since an ELDOR effect arises from spectral diffusion, the absence of ELDOR signals at temperatures above 160 K shows that T_{1n} and T_{x1} are not significantly shorter than T_{1e} at temperatures above 160 K.

Comparison of Time Constants Obtained by Various Methods. Throughout the temperature range examined, the S-band data fit well to a single exponential and the time constant was assigned as T_{1e}. Below about 30 K and above about 125 K, X-band CW-SR curves for the 4-Me-2,6-*t*-Bu-phenoxy radical fit well to single exponentials, and the time constant was assigned as T_{1e}. Above about 125 K the inversion recovery curves obtained with $B_1 = 3.0$ or 6.0 G and ED-SR could be fit to a single exponential, and the time constant agreed with the values obtained by CW-SR, consistent with $T_{1e} < T_{x1}, T_{1n}$ and consistent with the absence of an ELDOR effect. Above about 200 K even the inversion recovery curve obtained with $B_1 = 1.5$ G gave a time constant that agreed with the CW-SR value, indicating that $T_{1e} \leq T_s$. Since T_{1e} at this temperature is 20 μs, this comparison provides an estimate of a lower limit for T_s for this sample.

Between 35 and 125 K the CW-SR curves did not fit well to a single exponential. On the basis of the ELDOR data at 77 K and above, the fast component in the CW-SR curves is attributed to T_{x1}. The inversion recovery curves between 77 and 170 K were dependent on B_1, which indicates $T_s < T_{1e}$. The inversion recovery curves fit well to a sum of exponentials, but the components could not be clearly identified with individual processes.

Temperature Dependence of T_{1e}. The temperature dependence of T_{1e} for the 4-Me-2,6-*t*-Bu- phenoxy radical (Figure 10) below 100 K is dramatically different from that for the 2,4,6-*t*-Bu-phenoxy radical (Figure 3). The maximum in $1/T_{1e}$ at lower

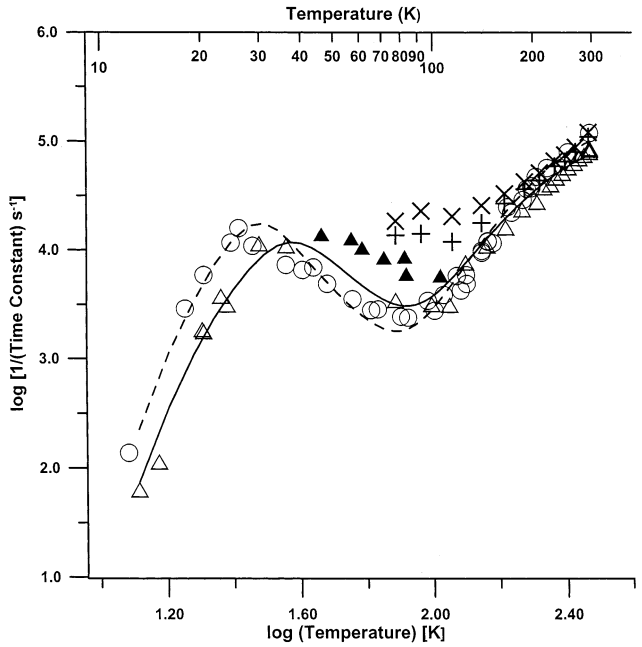

Figure 10. Temperature dependence of the recovery rate constants for 4-Me-2,6-*t*-Bu-phenoxy radical obtained by (×) X-band inversion recovery with $B_1 = 3.0$ G, (+) X-band ED-SR, (◇) X-band CW-SR or ELDOR, (○) S-band CW-SR, and (▲) CW-SR in the temperature region where time constants were shorter than obtained by ELDOR and therefore were not included in the fitting. (−) Fit to the X-band data, (- - -) fit to the S-band CW-SR data. The fit parameters are summarized in Table 1.

temperature at S-band than at X-band is characteristic of the effects of methyl rotation occurring at a rate comparable to the electron Larmor frequency. The fit lines in Figure 10 were obtained with $E_a = 165$ K (1.4 kJ) and a Davidson-Cole distribution parameter $\epsilon = 0.68$. This activation energy is somewhat lower than the literature values of 270 to 380 K for classical rotation (2.4 to 3.2 kJ).[17,43,44,74] The effects of methyl rotation on T_{1e} extend into the temperature range where tunneling dominates.[18,75] The tunneling barrier height is 230 to 320 K (2.0 to 2.8 kJ). Modeling the temperature dependence of $1/T_{1e}$ for the 4-Me-2,6-*t*-Bu-phenoxy radical between 10 and 80 K with $E_a = 190$ and 300 K gave a fit line that was similar to the one shown in Figure 10. These two activation energies could be viewed as an approximate analysis of the contribution from a tunneling process, in addition to classical rotation.

Above about 100 K, the values of $1/T_{1e}$ for 4-Me-2,6-*t*-Bu-phenoxy radical (Figure 10) are similar at X-band and S-band and are similar to the values for 2,4,6-*t*-Bu-phenoxy radical (Figure 3). Two-pulse spin−echo dephasing time constants, T_m, for the 4-Me-2,6-*t*-Bu-phenoxy radical were strongly temperature dependent between 77 and 295 K, with minimum values near 120 and 250 K. The strong temperature dependence of T_m indicates that methyls in the *tert*-butyl groups are rotating with rates comparable to the inequivalences in proton hyperfine couplings. The observation of two minima in T_m shows that the differences in barriers to rotation for different types of methyls are greater for the 4-methyl phenoxy radical than for the 4-*tert*-butyl analogue. Analysis of the temperature dependence of NMR T_1 values for nonirradiated 4-Me-2,6-*t*-Bu-phenol found $E_a = 9.88$ kJ (1180 K) and 34.4 kJ (4100 K) for nonequivalent methyls.[76,77] An ENDOR study found $E_a = 10.48$ kJ (1250 K) and 20.8 kJ (2480 K) for the *tert*-butyl methyl groups in the 4-Me-2,6-*t*-Bu-phenoxy radical.[78] An average of the literature values for the faster-rotating methyl groups ($E_a =$ 1200 K) was used to fit the temperature dependence of $1/T_{1e}$ for the 4-Me-2,6-*t*-Bu-phenoxy radical above 100 K (Figure 10). The methyls that give rise to the minimum in T_m at about 250 K (and presumably correspond to the literature activation energies of 3000 to 4000 K) are likely to be rotating too slowly to impact T_{1e} within the temperature range examined. The larger difference between the relaxation times at X-band and S-band for the 2,4,6-*t*-Bu-phenoxy radical (Figure 3) than for the 4-Me-2,6-*t*-Bu-phenoxy radical (Figure 10) above about 100 K is attributed to larger spin density on the 4-*tert*-butyl group than on the 2- or 6-*tert*-butyl groups.

Discussion

For radicals in irradiated glycylglycine, L-alanine, and 4-Me-2,6-*t*-Bu-phenol, different recovery time constants were obtained by inversion recovery, ED-SR, and long-pump CW-SR at some temperatures, which indicates the importance of spectral diffusion processes. Any process that transfers magnetization out of the observation bandwidth may contribute to the recovery curve. The observation bandwidth depends on the experiment performed. If the time constant for a spectral diffusion process is shorter than T_{1e}, but long enough to be observable, the apparent time constant for return to equilibrium will be shorter than T_{1e}. However, if the pump time that is used to excite a spin transition is longer than T_{1e}, the contribution of spectral diffusion processes to the observed recovery curve can in some cases be decreased.

For the 2,4,6-tri-*t*-Bu-phenoxy radical, which has a single-line EPR spectrum, the recovery curves from each of the experiments could be fit to a single exponential and the time constant obtained by the three techniques agreed well (Figure 3). On the basis of these observations, we conclude that spectral diffusion did not make a significant contribution to the recovery curves and the time constants obtained by any of the methods for 2,4,6-tri-*t*-Bu-phenoxy radical can be equated with T_{1e}.

For the radicals with EPR spectra that exhibited resolved hyperfine splittings (Figure 1), spectral diffusion caused the recovery time constants calculated from single exponential fits to inversion recovery and/or ED-SR curves to be significantly shorter than T_{1e} obtained by CW-SR or ELDOR (Figures 4, 7, and 10). ELDOR experiments and measurements of inversion recovery time constants as a function of B_1 were used to characterize three spectral diffusion processes: spin diffusion, nuclear spin relaxation, and cross relaxation.

Of the samples studied, the 2,4,6-*t*-Bu-phenoxy radical has the narrowest line, so at $B_1 = 6.0$ G a large fraction of the spins are excited, and spin diffusion has negligible effects. For the other samples, even at $B_1 = 6.0$ G, a relatively small fraction of the spectrum was excited and spin diffusion made substantial contributions to the inversion recovery curves at temperatures where $T_s < T_{1e}$. T_s does not exhibit substantial temperature dependence, as expected for a dipolar mechanism,[79] and was of the order of 1 to 10 μs. Because of uncertainties in the relative populations of spins that participate in spin diffusion (the population of the spin diffusion bath, Figure 2) it is difficult to determine precise values for T_s. The 6 μs pump of the ED-SR was long enough to substantially mitigate the impact of spin diffusion for the 2,4,6-*t*-Bu-phenoxy radical (Figure 10). CW-SR pump times longer than T_s effectively eliminated its contribution to the recovery curves.

For the two radicals with resolved hyperfine coupling to a unique proton, the glycylglycine radical and the radical in irradiated L-alanine, ELDOR reductions were observed in temperature ranges where $T_{1n} \leq T_{1e}$. For glycylglycine, T_{1n} is

approximately independent of temperature between 112 and 295 K, and is substantially shorter than T_{1e} over much of this temperature interval. For L-alanine, $T_{1n} \sim T_{1e}$ between about 153 and 295 K (Figure 9). Between about 100 and 150 K, the rate of rotation of the methyl group in the radical is comparable to the proton hyperfine coupling, which moves magnetization between positions in the CW spectrum for irradiated L-alanine. The effects of this process on the relaxation curves are difficult to distinguish from T_{1n}. The effects of short T_{1n} on the CW-SR curves could be mitigated with pump times longer than T_{1n}. The glycylglycine radical has been suggested as a standard for measuring microwave B_1 at the sample using CW power saturation.[80] This study found $(T_1T_2)^{1/2} = 1.3 \times 10^{-6}$ s at 77 K and 4.0×10^{-7} s at 295 K. For small turning angles spin−echo measurement give $T_m \sim 0.3 \times 10^{-6}$ s for the glycylglycine radical at 295 K, so $T_2 \geq 0.3 \times 10^{-6}$ s. This value of T_2, and $T_{1e} = 53 \times 10^{-6}$ s at 295 K, gives $(T_1T_2)^{1/2} > 4 \times 10^{-6}$. The much longer values of the relaxation times obtained by the pulse techniques than by CW saturation suggest that the CW measurements were strongly impacted by spectral diffusion processes.

Rapid cross relaxation (short T_{x1}) was observed for irradiated L-alanine above about 220 K and for 4-Me-2,6-*t*-Bu-phenoxide radical between 77 and 125 K. For these samples, at temperatures for which $T_{x1} < T_{1e}$, the data suggest that even with long pump times, the time constants obtained by CW-SR are shorter than T_{1e} obtained by ELDOR. It has previously been noted that when there is efficient cross-relaxation, increasing SR pulse lengths may give a limiting relaxation time that still includes contributions from both T_{1e} and T_{x1}.[38,81] Efficient cross relaxation in irradiated L-alanine has been attributed to methyl groups rotating at frequencies near the Larmor frequency.[56,69,71] For irradiated L-alanine, the shortest T_{x1} and the maximum ELDOR enhancement occur at about 270 K,[17,57] which is higher than the temperature for the maximum effect of the methyl groups on T_{1e}, and suggests that lattice methyl groups may contribute to the cross relaxation. The activation energy for rotation of lattice methyl groups is higher than for the methyl groups in the radical, so the lattice methyls enhance T_{x1} at higher temperatures than do the α-methyl groups in the radical.

The rate of rotation of the α-methyl group has dramatic effects on spin−echo dephasing ($1/T_m$) and transition energies for most of the EPR transitions for the L-alanine radical, but does not impact the transitions with the unpaired electron coupled to the (++++) or (− − − −) combination of proton nuclear spin states (lines 1 and 5 in Figure 1C). However, $1/T_m$ for these lines is temperature dependent above 77 K, characteristic of the effects of a dynamic process, which is attributed to averaging of weak dipolar couplings by rotation of lattice methyl groups at rates in the MHz range. These couplings are too small to be resolved relative to the ∼4 G widths of the partially resolved splittings of the proton hyperfine lines, so these dynamic effects have negligible effect on the CW line shapes. For barriers to rotation of the order of 1500 K, a relatively small change in temperature can cause the rate of rotation to go from the MHz to GHz range, so it is plausible that the lattice methyl groups that impact T_m above 77 K cause short T_{x1} above 200 K.

Processes that Contribute to Spin-Lattice Relaxation. The Raman process is independent of microwave frequency and produces a distinctive temperature dependence of T_{1e}. It dominates the relaxation between about 25 and 295 K for the glycylglycine radical (Figure 4), between 20 and 60 K for the 2,4,6-tri-*t*-Bu-phenoxy radical (Figure 3), and contributes between 30 and 100 K for the radical in L-alanine (Figure 7). The Debye temperatures used to fit the experimental data are 140 to 150 K, and the coefficients are $(1.8-4.3) \times 10^4$. These Debye temperatures are about a factor of 2 larger and the coefficients are about the same as for nitroxyl radicals in glassy solvents.[16] The weaker temperature dependence of T_{1e} for the glycylglycine radical below 20 K and for irradiated L-alanine below 30 K is attributed to the direct process or another process with similar temperature dependence involving electron−electron interaction.[1] The contribution from this process is larger for the irradiated L-alanine with 1.3×10^{19} spin/cm^3 than for the glycylglycine radical sample with 7.2×10^{18} spin/cm^3.

The distinctive temperature dependence of T_{1e} for irradiated L-alanine between about 100 and 250 K and for the 4-Me-2,6-*t*-Bu-phenoxy radical between 12 and 100 K is attributed to rotation of the unique methyl group in each radical. A characteristic of the contributions from these processes is the dependence of T_{1e} on microwave frequency (eq 1). The temperature dependence of T_{1e} for these samples was modeled to determine the activation energy for the rotation. For irradiated L-alanine an additional dynamic process dominates T_{1e} at higher temperatures, which is attributed to rotation of one or more neighboring methyl groups in the lattice.[82] The weaker couplings to methyls of the *tert*-butyl groups in 2,4,6-*t*-Bu-phenoxide and in 4-Me-2,6-*t*-Bu-phenoxide have smaller impacts on T_{1e} (Figures 3 and 10) than the methyl groups with coupling constants of 11 and 25 G in 4-Me-2,6-*t*-Bu-phenoxide and irradiated L-alanine, respectively (Figures 10 and 7). The magnitude of the effects of the weakly coupled methyl groups on T_{1e} in the phenoxy radicals is similar to the effects of the methyl groups in nitroxyl radicals.[16]

Conclusion

In the absence of rapid spectral diffusion processes, inversion recovery, ED-SR, CW-SR, and ELDOR experiments gave comparable values of T_{1e}. The longer pump times in the CW-SR experiments are more effective in minimizing the effects of spectral diffusion than the shorter pump times used in the ED-SR or inversion recovery experiments. However, even with long pump times, CW-SR experiments gave shorter time constants than the T_{1e} obtained by ELDOR experiments when there was rapid cross-relaxation. ELDOR experiments permitted characterization of the spectral diffusion processes (T_{1n} and T_{x1}) that move magnetization between resolved hyperfine lines. Rapid cross-relaxation was observed in samples with dipolar coupling to methyl groups rotating at rates comparable to the electron Larmor frequency.

The contributions to T_{1e} from the Raman process and local modes can be distinguished from thermally activated methyl group rotation by comparison of relaxation times at S-band and X-band. Rotation of *tert*-butyl methyl groups, which have small couplings to the unpaired electron, have smaller effects on the relaxation than more strongly coupled methyl groups and these effects would be difficult to distinguish from a local vibrational mode if only X-band data had been considered. The activation energies for methyl rotation were determined by analysis of the temperature dependence of T_{1e}.

Acknowledgment. Support of this work by NIH grant GM21156 is gratefully acknowledged. We thank Cobe Laboratories (Golden, CO) for irradiating the samples. Robert J. S. Brown (Claremont, CA) graciously provided the source code for the UPEN routines. Prof. George Rinard assisted in the development of the Mathcad routines based on the model in Figure 2B. Richard Quine wrote the software to implement the

programmable timing unit for the pulse sequences used in these experiments.

Appendix

Simultaneous equations that define the time dependence of the populations of the 8 energy levels drawn in Figure 2A.

$$\frac{dn_1}{dt} = -W_e[(n_1 - N_1) - (n_2 - N_2)] - W_N(n_1 - n_3) - W_{x1}[(n_1 - N_1) - (n_4 - N_4)] - W_s\left[(n_1 - N_1) - \frac{1}{P}(n_5 - N_5)\right]$$

$$\frac{dn_2}{dt} = +W_e[(n_1 - N_1) - (n_2 - N_2)] - W_N(n_2 - n_4) - W_{x2}[(n_2 - N_2) - (n_3 - N_3)] - W_s\left[(n_2 - N_2) - \frac{1}{P}(n_6 - N_6)\right]$$

$$\frac{dn_3}{dt} = -W_e[(n_3 - N_3) - (n_4 - N_4)] - W_N(n_3 - n_1) - W_{x2}[(n_3 - N_3) - (n_2 - N_2)] - W_s\left[(n_3 - N_3) - \frac{1}{P}(n_7 - N_7)\right]$$

$$\frac{dn_4}{dt} = +W_e[(n_3 - N_3) - (n_4 - N_4)] - W_N(n_4 - n_2) - W_{x1}[(n_4 - N_4) - (n_1 - N_1)] - W_s\left[(n_4 - N_4) - \frac{1}{P}(n_8 - N_8)\right]$$

$$\frac{dn_5}{dt} = -W_e[(n_5 - N_5) - (n_6 - N_6)] - W_N(n_5 - n_7) - W_{x1}[(n_5 - N_5) - (n_8 - N_8)] + W_s\left[(n_1 - N_1) - \frac{1}{P}(n_5 - N_5)\right]$$

$$\frac{dn_6}{dt} = +W_e[(n_5 - N_5) - (n_6 - N_6)] - W_N(n_6 - n_8) - W_{x2}[(n_6 - N_6) - (n_7 - N_7)] + W_s\left[(n_2 - N_2) - \frac{1}{P}(n_6 - N_6)\right]$$

$$\frac{dn_7}{dt} = -W_e[(n_7 - N_7) - (n_8 - N_8)] - W_N(n_7 - n_5) - W_{x2}[(n_7 - N_7) - (n_6 - N_6)] + W_s\left[(n_3 - N_3) - \frac{1}{P}(n_7 - N_7)\right]$$

$$\frac{dn_8}{dt} = +W_e[(n_7 - N_7) - (n_8 - N_8)] - W_N(n_8 - n_6) - W_{x1}[(n_8 - N_8) - (n_5 - N_5)] + W_s\left[(n_4 - N_4) - \frac{1}{P}(n_8 - N_8)\right]$$

where

$$W_e = \frac{1}{2T_{1e}}; \quad W_N = \frac{1}{2T_{1n}}; \quad W_{x1} = \frac{1}{2T_{x1}}; \quad W_{x2} = \frac{1}{2T_{x2}}; \quad W_s = \frac{1}{2T_s}$$

and n_i is the instantaneous population of energy level i; N_i is the equilibrium population of energy level i; and P is the relative population of the spin diffusion bath.

To expand the model to include 8 energy levels and 8 corresponding spin baths (the energy level scheme schown in Figure 2B), the following parameters are added: P_j with j = A,B,C,D represents the relative intensity of the 4 hyperfine lines; f_{ij} with ij = AB, BC, or CD, represents the number of possible combinations of spin flips that could interconvert hyperfine lines i and j. P_s is the population of the spin diffusion bath. For example dn_1/dt becomes

$$\frac{dn_1}{dt} = -W_e\left[\frac{(n_1 - N_1)}{P_A} - \frac{(n_2 - N_2)}{P_A}\right] - W_N f_{AB}\left[\frac{(n_1 - N_1)}{P_A} - \frac{(n_3 - N_3)}{P_B}\right] - W_{x1} f_{AB}\left[\frac{(n_1 - N_1)}{P_A} - \frac{(n_4 - N_4)}{P_B}\right] - W_s f_s\left[\left(\frac{n_1 - N_1}{P_A}\right) - \left(\frac{n_9 - N_9}{P_s}\right)\right]$$

References and Notes

(1) For example, see the following articles and references therein: (a) Eaton, S. S.; Eaton, G. R. *Biol. Magn. Reson.* **2000**, *19*, 29−154. (b) Eaton, S. S.; Eaton, G. R. *Biol. Magn. Reson.* **2000**, *19*, 348−381. (c) Lakshmi, K. V.; Brudvig, G. W. *Biol. Magn. Reson.* **2000**, *19*, 513−567.

(2) Idziak, S.; Pislewski, N. *Chem. Phys.* **1987**, *111*, 439−443.

(3) Andrew, E. R.; Hinshaw, W. S.; Hutchins, M. G.; Sjoblom, R. O. S.; Canepa, P. C. *Mol. Phys.* **1976**, *32*, 795−806.

(4) Beckmann, P. A.; Fusco, F. A.; O'Neill, A. E. *J. Magn. Reson.* **1984**, *59*, 63−70.

(5) Beckmann, P. A.; Al-Hallaq, H. A.; Fry, A. M.; Plofker, A. L.; Roe, B. A. *J. Chem. Phys.* **1994**, *100*, 752−753.

(6) Beckmann, P. A.; Hill, A. I.; Kohler, E. B.; Yu, H. *Phys. Rev. B* **1988**, *38*, 11098−11111.

(7) Andrew, E. R.; Hinshaw, W. S.; Hutchins, M. G. *J. Magn. Reson.* **1974**, *15*, 196−200.

(8) Standley, K. J.; Vaughn, R. A. *Electron Spin Relaxation Phenomena in Solids*; Plenum Press: New York, 1969.

(9) Abragam, A.; Bleaney, B. *Electron Paramagnetic Resonance of Transition Ions*; Oxford University Press: London, 1970.

(10) Bertini, I.; Martini, G.; Luchinat, C. In *Handbook of Electron Spin Resonance*; Poole, C. P., Jr., Farach, H., Eds.; American Institute of Physics: New York, 1994; pp 51−77.

(11) Scholes, C. P.; Isaacson, R. A.; Feyer, G. *Biochim. Biophys. Acta* **1971**, *244*, 206−210.

(12) Yim, M. B.; Kuo, L. C.; Makinen, M. W. *J. Magn. Reson.* **1982**, *46*, 247−256.

(13) Makinen, M. W.; Yim, M. B. *Proc. Natl. Acad. Sci. U.S.A.* **1981**, *78*, 6221−6225.

(14) Makinen, M. W.; Wells, G. B. *Metal Ions Biol. Syst.* **1987**, *22*, 129−206.

(15) Orton, J. W. *Electron Paramagnetic Resonance*; Gordon and Breach: New York, 1968.

(16) Zhou, Y.; Bowler, B. E.; Eaton, G. R.; Eaton, S. S. *J. Magn. Reson.* **1999**, *139*, 165−174.

(17) Brustolon, M.; Cassol, T.; Micheletti, L.; Segre, U. *Mol. Phys.* **1986**, *57*, 1005−1014.

(18) Clough, S.; Poldy, F. *J. Chem. Phys.* **1969**, *51*, 2076−2084.

(19) Feldman, D. W.; Castle, J. G., Jr.; Wagner, G. R. *Phys. Rev.* **1966**, *145*, 237−240.

(20) Castle, J. G., Jr.; Feldman, D. W. *Phys. Rev. A* **1965**, *137*, 671−673.

(21) Castle, J. G., Jr.; Feldman, D. W. *J. Appl. Phys.* **1965**, *36*, 124−128.

(22) Muromtsev, V. I.; Shteinshneider, N. Ya.; Safranov, S. N.; Golikov, V. P.; Kuznetsov, A. I.; Zhidomirov, G. M. *Fiz. Tverd. Tela* **1975**, *17*, 813−814 (pp 517−519 in transl.).

(23) Kivelson, D. *J. Chem. Phys.* **1960**, *33*, 1094−1106.

(24) Wilson, R.; Kivelson, D. *J. Chem. Phys.* **1966**, *44*, 154−168.

(25) Du, J.-L.; Eaton, G. R.; Eaton, S. S. *J. Magn. Reson. A* **1996**, *119*, 240−246.

(26) Salikov, K. M.; Tsvetkov, Yu. D. In *Time Domain Electron Spin Resonance*; Kevan, L., Schwartz, R. N., Eds.; Wiley: New York, 1979; pp 231−277.

(27) Bowman, M. K.; Kevan, L. In *Time Domain Electron Spin Resonance*; Kevan, L., Schwartz, R. N., Eds.; Wiley: New York, 1979; pp 68−105.

(28) Anderson, P. W. *Phys. Rev.* **1958**, *109*, 1492−1505.

(29) Wolf, E. L. *Phys. Rev.* **1966**, *142*, 555−569.

(30) Tse, D.; Hartmann, S. R. *Phys. Rev. Lett.* **1968**, *21*, 511−514.

(31) Eaton, S. S.; Eaton, G. R. *J. Magn. Reson. A* **1993**, *102*, 354−356.

(32) Blombergen, N. *Physica* **1949**, *15*, 386−426.

(33) Wenckebach, W. Th.; Poulis, N. J. *17th Congress Ampere*; Hovi, V., Ed.; North-Holland Pub.: Amsterdam, 1973; pp 120−142.

(34) Bowman, M. K.; Kevan, L. *Discuss. Faraday Soc.* **1977**, *63*, 7−17.
(35) Bowman, M. K.; Norris, J. R. *J. Phys. Chem.* **1982**, *86*, 3385−3390.
(36) Kevan, L.; Narayana, P. A In *Multiple Electron Resonance Spectroscopy*; Dorio, M. N., Freed, J. H., Eds.; Plenum Press: New York, 1979; pp 288−298.
(37) Manenkov, A. A.; Pol'skii, Yu. E. *Sov. Phys. JETP* **1963**, *45*, 1425−1429. (**1964**, *18*, 985−987 in transl.).
(38) Manenkov, A. A.; Prokhorov, A. M. *Sov. Phys. JETP* **1962**, *42*, 75−83. (pp 54−59 in transl.).
(39) Manenkov, A. A.; Milyaev, V. A.; Prokhorov, A. M. *Sov. Phys. Solid State* **1962**, *4*, 388−391 (pp 280−283 in transl.).
(40) Yamauchi, J.; Katayama, A.; Tamada, M.; Tanaka, M. S. *Appl. Magn. Reson.* **2000**, *18*, 249−254.
(41) Lin, W. C.; McDowell, C. A. *Mol. Phys.* **1961**, *4*, 333−342.
(42) Katayama, M.; Gordy, W. *J. Chem. Phys.* **1961**, *35*, 117−122.
(43) Clough, S.; Mulandy, B. J. *Phys. Rev. Lett.* **1973**, *30*, 161−163.
(44) Bonon, F.; Brustolon, M.; Maniero, A. L.; Segre, U. In *Electron Spin Resonance (ESR) Applications in Organic and Bioorganic Materials*; Catoire, B., Ed.; Springer-Verlag: New York, 1992; pp 285−289.
(45) Krushev, V. V.; Koizumi, H.; Ichikawa, T.; Yoshida, H.; Shibata, H.; Tagawa, S.; Wilkens, B. *J. Radiat. Phys. Chem.* **1994**, *44*, 521−526.
(46) Harbridge, J. R.; Rinard, G. A.; Quine, R. W.; Eaton, S. S.; Eaton, G. R. *J. Magn. Reson.* **2002**, *156*, 1−11.
(47) Zecevic, A.; Eaton, G. R.; Eaton, S. S.; Lindgren, M. *Mol. Phys.* **1998**, *95*, 1255−1263.
(48) Quine, R. W.; Eaton, S. S.; Eaton, G. R. *Rev. Sci. Instrum.* **1992**, *63*, 4251−4262.
(49) Rinard, G. A.; Quine, R. W.; Song, R.; Eaton, G. R.; Eaton, S. S. *J. Magn. Reson.* **1999**, *140*, 69−83.
(50) Rinard, G. A.; Quine, R. W.; Ghim, B. T.; Eaton, S. S.; Eaton, G. R. *J. Magn. Reson.* **1996**, *122*, 50−57.
(51) Quine, R. W.; Eaton, G. R.; Eaton, S. S. *Rev. Sci. Instrum.* **1987**, *58*, 1709−1724.
(52) Rinard, G. A.; Quine, R. W.; Harbridge, J. R.; Song, R.; Eaton, G. R.; Eaton, S. S. *J. Magn. Reson.* **1999**, *140*, 218−227.
(53) Provencher, S. W. *J. Chem. Phys.* **1976**, *64*, 2772−2777.
(54) Borgia, G. C.; Brown, R. J. S.; Fantazzini, P. *J. Magn. Reson.* **1998**, *132*, 65−77.
(55) Borgia, G. C.; Brown, R. J. S.; Fantazzini, P. *J. Magn. Reson.* **2000**, *147*, 273−285.
(56) Rakvin, B.; Maltar-Strmecki, N.; Cevc, P.; Arcon, D. *J. Magn. Reson.* **2001**, *152*, 149−155.
(57) Angelone, R.; Forte, C.; Pinzino, C. *J. Magn. Reson.* **1993**, *101*, 16−22.
(58) Hyde, J. S.; Chien, J. C. W.; Freed, J. H. *J. Chem. Phys.* **1968**, *48*, 4211−4226.
(59) Nechtschein, M.; Hyde, J. S. *Phys. Rev. Lett.* **1970**, *24*, 672−674.
(60) Abragam, A. *The Principles of Nuclear Magnetism*; Oxford University Press: London, 1961; pp 405−409.
(61) Murphy, J. *Phys. Rev.* **1966**, *145*, 241−247.
(62) Atsarkin, V. A.; Demidov, V. V.; Vasneva, G. A. *Phys. Rev. B* **1997**, *56*, 9448−9453.
(63) Beckmann, P. A. *Phys. Rep.* **1988**, *171*, 85−128.
(64) Forrester, A. R.; Hay, J. M.; Thomson, R. H. *Organic Chemistry of Stable Free Radicals*; Academic Press: New York, 1968; Chapter 7; and Landolt-Bornstein, 17th ed.; Berlin: Springer, 1988.
(65) Miyagawa, I.; Gordy, W. *J. Chem. Phys.* **1960**, *32*, 255−263.
(66) Regulla, D. F.; Defner, U. *Int. J. Appl. Radiat. Isot.* **1982**, *33*, 1101−1114.
(67) Nagy, V.; Sleptchonok, O. F.; Desrosiers, M. F.; Weber, R. T.; Heiss, A. H. *Radiat. Phys. Chem.* **2000**, *59*, 429−441.
(68) Miyagawa, I.; Itoh, K. *J. Chem. Phys.* **1962**, *36*, 2157−2163.
(69) Rakvin, B.; Maltar-Strmecki, N. *Spectrosc. Acta* **2000**, *56*, 399−408.
(70) Kispert, L. D.; Chang, K.; Bogan, C. M *J. Chem. Phys.* **1973**, *58*, 2164−2176.
(71) Dzuba, S. A.; Salikhov, K. M.; Tsvetkov, Yu. D. *Chem. Phys. Lett.* **1981**, *79*, 568−572.
(72) Ghim, B. T.; Du, J.; Pfenninger, S.; Rinard, G. A.; Quine, R. W.; Eaton, S. S.; Eaton, G. R. *Appl. Radiat. Isot.* **1996**, *47*, 1235−1239.
(73) Becconsall, J. K.; Clough, S.; Scott, G. *Trans. Faraday Soc.* **1960**, *56*, 459−472.
(74) Clough, S.; Heidemann, A. *J. Phys. C: Solid State Phys.* **1980**, *13*, 3585−3589.
(75) Clough, S.; Heidemann, A.; Horsewill, A. J.; Lewis, J. D.; Paley, M. N. J. *J. Phys. C: Solid State Phys.* **1982**, *15*, 2495−2508.
(76) Beckmann, P. A.; Ratcliffe, C. I.; Dunell, B. A. *J. Magn. Reson.* **1978**, *32*, 391−402.
(77) Beckmann, P. A.; Fusco, F. A.; O'Neill, A. E. *J. Magn. Reson.* **1984**, *59*, 63−70.
(78) Brustolon, M.; Maniero, A. L.; Bonoro, M.; Segre, U. *Appl. Magn. Reson.* **1996**, *11*, 99−113.
(79) Diezemann, G. *J. Chem. Phys.* **1995**, *103*, 6368−6384.
(80) Copeland, E. S. *Rev. Sci. Instrum.* **1973**, *44*, 437−442.
(81) Manenkov, A. A.; Milyaev, V. A. *Sov. Phys. JETP* **1970**, *31*, 427−428.
(82) Kuroda, S.; Miyagawa, I. *J. Chem. Phys.* **1982**, *76*, 3933−3944.